3

Finite element analysis of composite forming

P BOISSE, INSA de Lyon, France

3.1 Introduction: finite element analyses of composite forming, why and where?

The finite element (FE) method is a relatively recent approach (Argyris, 1960) to finding numerical solutions to physical problems, especially in the field of solid and fluid mechanics. The method has been extended to some manufacturing process simulations, in particular to metal forming (Wagoner *et al.*, 1996) and crash simulation (Halquist *et al.*, 1985). Commercial software packages have been developed that allow fairly efficient analyses for industrial cases. The FE method often requires lengthy computation times, especially in manufacturing process simulations, but advances in computer efficiency make this drawback less important. The FE method is currently the most commonly used numerical approach, but several other numerical methods (such as the Natural Element Method (NEM) and Smooth Particle Hydrodynamics (SPH) (Sukumar *et al.*, 1998; Gingold *et al.*, 1977)) have appeared or are being developed. All these methods have the same goal, which is to give an approximated numerical solution to a global physical problem from its governing equations.

The most commonly used approach for analysing composite forming processes, and especially draping in woven composite reinforcements, is 'kinematical models' (Mark *et al.*, 1956; Van Der Ween, 1991; Long *et al.*, 1994; Borouchaki *et al.*, 2003). Several packages are commercially available, such as FiberSIM and ESI-QuickFORM. This method is fairly efficient for hand draping in classical prepreg fabrics, but the models do not account for load boundary conditions, for possible sliding of the fabric in relation to the tools, or the mechanical behaviour of the woven reinforcement, although constitutive aspects have been introduced in some approaches (Long *et al.*, 2001).

For a physical (or mechanical) analysis of a composite forming process, the complete model must include all the equations for the mechanics, especially equilibrium, constitutive equations, and boundary conditions. These equations must be solved numerically, with some approximations. Finite element analysis of the composite forming process includes modelling the tools, the contact and

friction between the different parts, and above all, the mechanical behaviour of the composite during forming. As mentioned above, problems of computation time are reduced through improved processing capabilities. Better optimisation of methods has also improved efficiency. The main problem for the FE approach therefore lies in the requirement for accurate models of all the significant aspects of the forming process. When the models are defined and implemented, an FE analysis of a composite process gives detailed results concerning all the fields of unknowns, such as displacement, strain, stress, tensions in the yarns, and temperature, for any time during the process.

There are two main reasons for simulating the composite forming process. The first concerns the process itself and its feasibility. The simulation can give the conditions (for instance loads on the tools, initial orientation, type of material, etc.) that will make the forming possible, and also describe any possible defects after forming (wrinkles, porosities, yarn fractures, etc.). This is similar to simulating metal forming. Secondly, and unique to composite forming analysis, is the need to know at any point the directions and density of the fibres after forming. A woven composite reinforcement can be formed on a double curved shape because of the angle variations between warp and weft yarns, i.e. the in-plane shear strains. These angle variations can be very large, up to 50º, consequently the yarn directions depend significantly on the forming process. The directions and densities of fibres are also very important for analysing how the composite part will behave in use, with regards to stiffness, damage, fatigue, etc.

Fabric draping is not the only field in composite forming where FE analysis is used. Another important field for composite manufacturing simulations concerns mould filling in liquid composite moulding. In these processes, a liquid resin is injected through a fibrous reinforcement that has been shaped previously in the mould. Simulation of mould filling is usually based on the Darcy law (Darcy, 1856), associated with FE (or/and finite volume) approximations (Trochu *et al.*, 1993; Breard *et al.*, 2005; Comas-Cardona *et al.*, 2005). This flow analysis is mainly influenced by draping, when the part is double curved, because the permeability depends strongly on the angle between warp and weft yarns (Fournier *et al.*, 2005).

Although the above descriptions concern FE analysis of the entire composite forming process, because of the multiscale nature of composites, it is necessary to compute phenomena at lower scales. Analysing the deformations of a woven unit cell permits us to understand and identify the mechanical properties of the fabric as a whole (Boisse *et al.*, 2001; Hagège *et al.*, 2005; Lomov *et al.*, 2005), and resin flow simulations in this woven unit determine the permeability overall (Fournier *et al.*, 2005; Laine *et al.*, 2005). This chapter will focus on FE analysis of composite reinforcement forming.

3.2 The multiscale nature of composite materials and different approaches for composite forming simulations

3.2.1 Multiscale materials

Composite materials are made of fibres and matrix, and the fibre arrangements are numerous. Fibres can be short (SMC, BMC, GMT, etc.) or continuous, as is the case for composite structures that must withstand strong loads. Continuous fibres can be simply juxtaposed, or unidirectional (UD), woven, juxtaposed and stitched (non-crimp fabrics, NCF), braided, knitted or randomly oriented (mats). The arrangement of fibres is very important and the materials resulting from the various arrangements are very different. Composite materials are typically multiscale materials because the architecture and the properties at lower scales strongly influence the behaviour of the composite. This is true for composites during use, but it is even more the case in the forming process because the lack of matrix (or of matrix efficiency) renders the internal reinforcement architecture more essential.

Three scales can generally be distinguished in composite reinforcements. The macroscopic scale is that of the composite part for which the forming is being studied. The mesoscopic scale is an intermediate scale that concerns the yarn architecture. Typically, it is the scale of the unit woven cell, or knitted cell in the case of textile composites. Finally, the microscopic scale is that relating to the numerous fibres that make up the yarns (or tows or bundles), for instance a carbon yarn may contain 6000 fibres (in the case of the yarn in Fig. 3.14). The arrangement and density of the fibres within the yarn affect its behaviour. Fibre diameters for carbon, glass, aramid, polypropylene, etc., are usually between 5 μm and 50 μm.

3.2.2 Mechanism and specificity of composite forming

It is necessary to distinguish between composites with short fibres and composites with continuous fibres. Short fibres improve the mechanical properties of a material through the matrix, but this matrix remains the basic element. Injection is one of the manufacturing technologies used for materials with short fibres. The forming simulation in this case is a resin flow problem, but with fibres that are oriented by the forming (Dumont *et al.*, 2003; Chinesta *et al.*, 2005). In the case of continuous fibrous reinforcements, the reinforcements play a major role in the mechanical behaviour of the composite, the main function of the matrix being to prevent relative displacements of continuous filaments. This type of composite is used where load-bearing is important. The forming of composites with continuous reinforcements will be analysed below.

Forming of composite materials differs from that of materials such as metals or polymers because it uses the fibre-matrix composition of the composite. The forming process is performed in a state in which the matrix does not play a role.

In Liquid Composite Moulding (LCM) processes, the reinforcement is shaped before the resin is injected. Bending and in-plane shear are possible, thus double curved shapes can be obtained. In the case of thermoset prepreg draping, the matrix is present but is not solid because it is not yet polymerised, thus the reinforcement can be deformed as well. For Continuous Fibres Reinforced Thermoplastics (CFRTP) prepregs forming, the matrix is heated above the melting temperature, and this permits deformation of the reinforcement as well as the final forming. In these examples, the matrix is lacking or very weak and the internal architecture of the fibrous reinforcement permits the forming to take place. This is specific to composite materials and the forming modes are quite different to those of metals. There are usually very small extensions in the fibre directions, and the in-plane shear strains play a major role in forming. Codes for simulating the composite forming process and the approaches that are used are therefore specific to those materials.

3.2.3 Different approaches to FE analysis of composite forming

As described above, FE analysis of composite forming requires all the different aspects involved in the process to be modelled, in particular that of the fibrous reinforcement. This reinforcement can be with or without matrix, but as discussed in Section 3.2.2, this matrix is weak and allows the reinforcement to deform. The multiscale nature of the composite and of its fibrous reinforcement means that there are different possible approaches for FE analysis of the forming process.

The first approach considers the fibrous reinforcement as a continuum. The reinforcement is not continuous at lower scales, but that is the case for most materials under large strains (for instance a metal in plasticity), and a continuous material superimposed on the fibrous material can be postulated. This makes the assumption that there is no significant sliding between the fibres, i.e. that two neighbouring points in the initial state remain close after forming, which can be verified experimentally for most usual reinforcements. For instance, Fig. 3.1 (Boisse, 1994) shows a fibre woven fabric formed on a hemispherical, i.e. a double curve, shape. A set of lines following the warp and weft directions have been drawn on the fabric prior to forming. These lines become strongly curved after forming but remain continuous, which implies that, due to the weaving, there is no large sliding between warp and weft yarns (if there was, the lines would have become discontinuous), and consequently that the continuous approach is possible. The advantage of the continuous approach is that it can be used in standard finite elements, although the constitutive model of the continuum will have to convey the very specific mechanical behaviour of the fibrous reinforcement. Such behaviour depends mainly on the fibre directions, which change strongly during forming. Section 3.3 will demonstrate why the approaches normally used for anisotropic metal forming cannot be used here.

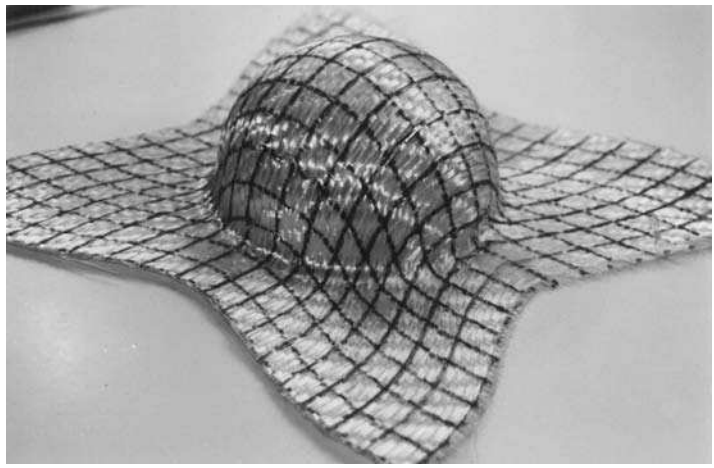

3.1 Deformation of straight lines drawn on the fabric prior to forming.

Other specific aspects of fibrous reinforcement mechanical behaviours, such as crimp change and shear locking, should also be taken into account in the model.

The opposite approach is to see the fibrous reinforcement as a set of elements at lower scales, such as the yarns, woven cells, fibres, etc. The FE analysis is then concerned with those elements that are in contact or are linked by springs. Although some approaches at the microscopic scale exist (Durville, 2002; Duhovic *et al.*, 2006), the large number of filaments means that it is more realistic to analyse a small number of elements at the mesoscale (woven or knitted cells, for instance), and it is not currently possible to analyse an entire forming process. The advantage over the continuous approach is that the description of the internal structure of the reinforcement naturally accounts for some aspects of the material, such as the directions of the fibres. Nevertheless, it is difficult to delineate models that are efficient enough at the mesoscale but simple enough to be able to analyse a forming process. Continuous and mesoscopic FE models are discussed in the next two sections.

3.3 The continuous approach for composite forming process analysis

This approach assumes that the composite can be considered as a continuum media during forming, consequently the mechanics of continuous media can be used. This assumption is questionable, especially for stress. What is the stress in a woven fabric? A stress tensor is defined as a function that gives in any point P the stress vector $d\vec{F}/dS$ for any normal vector. This is not clear if P is a point within a woven fabric. It is therefore necessary to consider a continuous media that is not exactly equal to the fibrous reinforcement, but that is homogenous and has the same global mechanical behaviour. This is possible if (as seen in Section

3.2.3 and Fig. 3.1) large sliding between the yarns is minimal. This method also makes an approximation, and so the local quantities in the fibrous reinforcement are only those of the continuous media on average.

The main difficulty in using the continuous approach is to capture the effects of the fibre architecture and its evolution. There are many models (see Chapter 2). Most of them assume that the fibrous reinforcement is elastic while forming. That is usually true for extensions in the fibre directions, but not usually true in the other directions, such as in-plane shear, bending, and transverse compression. Nevertheless, the forming process is a more or less constant operation and making this assumption doesn't change the result of the analysis greatly.

Continuous behaviour models that capture macro-level phenomena at lower scales generally concern homogenisation, although homogenisation typically refers to techniques applied to a two-scale periodic material, in which the analysis of a unit cell reveals the properties of the homogenised material (Hsiao *et al.*, 1999; Peng *et al.*, 2002). This approach is elegant but requires lengthy computational times. Furthermore, extending it to non-linear problems is difficult. Three continuous approaches used in FE analysis are described below.

3.3.1 Hypoelastic model for fibrous materials

In this method, fibres are considered to have a single direction. Approaches traditionally developed in finite element codes (such as ABAQUS, for instance) for anisotropic metal at large strains are based on Jaumann corotational formulation (Dafalias, 1983; Gilormini *et al.*, 1993) or the Green-Naghdi approach (Dienes, 1979; Gilormini *et al.*, 1993). In these models, a rotation is used both to define an objective derivative for the hypoelastic law and to update the othotropic frame. The rotations used in Green-Naghdi and Jaumann derivatives are average rotations of the material. The polar rotation $\mathbf{R}$ is used in Green-Naghdi:

$$\mathbf{R} = \mathbf{F}\mathbf{U}^{-1} \tag{3.1}$$

where $\mathbf{F}$ is the deformation gradient and $\mathbf{U}$ is a symmetrical strain tensor. In the Jaumann approach, the rotation $\mathbf{Q}$ of the corotational frame is used. These well-known approaches cannot be used for a fibrous material under large strains because the update for the strong direction must follow the fibre direction strictly. Figure 3.2 shows the evolution of the orthotropic direction in a finite element analysis of the extension of a knitted fibrous material (Hagège, 2004). The analysis, using ABAQUS, uses the hypoelastic Green-Naghdi approach and it can be seen that the orthotropic direction does not follow the fibre direction.

The following approach uses the rotation of the fibre denoted Δ (Hagège, 2004; Hagège *et al.*, 2005). The initial orientation of the orthotropic axes $\{\boldsymbol{\kappa}^0\}$ is defined by a rotation tensor field $\mathbf{O}$ that transforms the unitary vectors of the global basis $\{\mathbf{G}\}$:

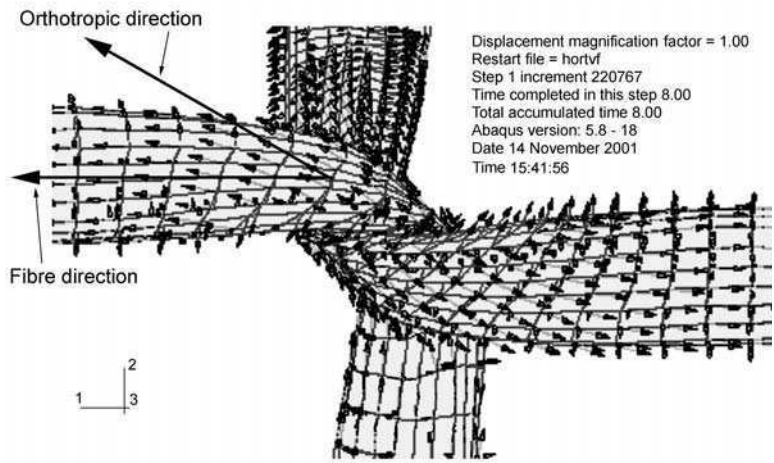

3.2 Orthotropic direction evolution in a Green-Naghdi analysis.

$$\boldsymbol{\kappa}_i^0 = \mathbf{O} \cdot \mathbf{G}_i \tag{3.2}$$

The material rotation $\boldsymbol{\Delta}$ is then used to update the initial constitutive axes $\{\boldsymbol{\kappa}^0\}$ to the current constitutive axes $\{\boldsymbol{\kappa}^t\}$ (Fig. 3.3):

$$\boldsymbol{\kappa}_i^t = \boldsymbol{\Delta} \cdot \boldsymbol{\kappa}_i^0 \tag{3.3}$$

Some developments of equation (3.3) (Criesfield, 1991) lead to equations (3.4) that explicitly give the constitutive axes $\{\boldsymbol{\kappa}^t\}$ as functions of the initial constitutive axes $\{\boldsymbol{\kappa}^0\}$ and the deformation gradient $\mathbf{F}$:

$$\begin{aligned}
\boldsymbol{\kappa}_1^t &= \frac{\mathbf{F} \cdot \boldsymbol{\kappa}_1^0}{\|\mathbf{F} \cdot \boldsymbol{\kappa}_1^0\|} \\
\boldsymbol{\kappa}_2^t &= \boldsymbol{\kappa}_2^0 - \frac{b_2}{1 + b_1}\left(\boldsymbol{\kappa}_1^0 + \boldsymbol{\kappa}_1^t\right) \\
\boldsymbol{\kappa}_3^t &= \boldsymbol{\kappa}_3^0 - \frac{b_3}{1 + b_1}\left(\boldsymbol{\kappa}_1^0 + \boldsymbol{\kappa}_1^t\right)
\end{aligned} \tag{3.4}$$

with $b_k = \boldsymbol{\kappa}_1^t \cdot \boldsymbol{\kappa}_k^0$ and $b_k \neq 1$. In this formulation, the fibre direction, i.e. the strong anisotropic direction, remains aligned with the first vector of $\{\boldsymbol{\kappa}^t\}$. The constitutive behaviour is then fully defined at each time point. In fact, the initial constitutive tensor ${}^0\mathbf{C}$ has known components that can be computed with the traditional engineer's constants:

$${}^0\mathbf{C} = {}^0\, C_{ijkl} \boldsymbol{\kappa}_i^0 \otimes \boldsymbol{\kappa}_j^0 \otimes \boldsymbol{\kappa}_k^0 \otimes \boldsymbol{\kappa}_l^0 \tag{3.5}$$

The current constitutive tensor $\mathbf{C}$ can be deduced from ${}^0\mathbf{C}$ by a rotational transport based on the fourth order rotation tensor Λ:

$$\mathbf{C} = \boldsymbol{\Lambda} : {}^0\mathbf{C} : \boldsymbol{\Lambda}^T \tag{3.6}$$

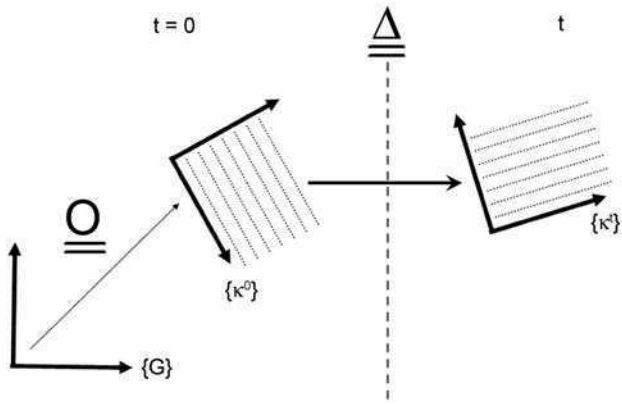

3.3 2D representation of the evolution of the constitutive axes $\{\boldsymbol{\kappa}^t\}$.

Λ is the fourth order rotational tensor obtained from $\boldsymbol{\Delta}$:

$$\forall \mathbf{A} \quad \boldsymbol{\Lambda} : \mathbf{A} = \boldsymbol{\Delta} \cdot \mathbf{A} \cdot \boldsymbol{\Delta}^T \tag{3.7}$$

Consequently $\mathbf{C}$ is given by:

$$\mathbf{C} = {}^0C_{ijkl} \boldsymbol{\kappa}_i^t \otimes \boldsymbol{\kappa}_j^t \otimes \boldsymbol{\kappa}_k^t \otimes \boldsymbol{\kappa}_l^t \tag{3.8}$$

The constitutive tensor $\mathbf{C}$ can be used in a hypo-elastic law written:

$$\boldsymbol{\sigma}^{\nabla} = \mathbf{C} : \mathbf{D} \tag{3.9}$$

$\mathbf{D}$ is the strain rate and $\boldsymbol{\sigma}^{\nabla}$ is the objective derivative of the Cauchy stress associated to the fibre rotation Δ.

$$\boldsymbol{\sigma}^{\nabla} = \boldsymbol{\Delta} \cdot \frac{d}{dt} \left(\boldsymbol{\Delta}^T \cdot \boldsymbol{\sigma} \cdot \boldsymbol{\Delta} \right) \cdot \boldsymbol{\Delta}^T \tag{3.10}$$

The cumulated tensorial strain tensor $\boldsymbol{\varepsilon}$ and stress tensor $\boldsymbol{\sigma}$ associated with such an objective derivative are given by:

$$\boldsymbol{\varepsilon} = \boldsymbol{\Delta} \cdot \left(\int_0^t \boldsymbol{\Delta}^T \cdot \mathbf{D} \cdot \boldsymbol{\Delta} \, dt \right) \cdot \boldsymbol{\Delta}^T \tag{3.11}$$

$$\boldsymbol{\sigma} = \boldsymbol{\Delta} \cdot \left(\int_0^t \boldsymbol{\Delta}^T \cdot \mathbf{C} \cdot \mathbf{D} \cdot \boldsymbol{\Delta} \, dt \right) \cdot \boldsymbol{\Delta}^T \tag{3.12}$$

It can be shown that equation (3.11) will always give a logarithmic strain in the strong anisotropic direction and that equation (3.12) ensures the summation of the stress increments along this direction.

Finally, the use of the material rotation tensor Δ for the objective derivative (3.10) and the evolution law (3.6) entails a consistent approach for fibrous media with one strong anisotropic direction. Figure 3.4 shows FE analysis of the same knitted material as Fig. 3.2, but uses the above approach implemented in

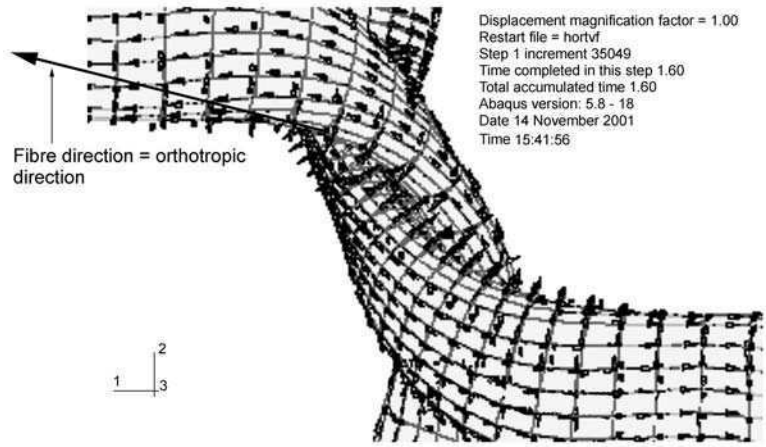

3.4 Orthotropic axes updated using the fibre rotation $\triangleq$.

ABAQUS via a VUMAT routine (User Material routine) (Hagège, 2004). In this case the orthotropic direction remains strictly in the fibre direction and it has been shown that the analysis is consistent with biaxial tension on knitted material (Hagège *et al.*, 2005).

The above approach is carried out for a single fibre direction, although many fibrous reinforcements, and especially woven fabrics, have two fibre directions. The behaviour here is no longer orthotropic because there are very large angle variations between the warp and weft directions due to in-plane shear. The above formulation can be used by superposition on the same point for two materials using their own fibre directions. Sliding between warp and weft directions can be ignored because the two materials (warp and weft) are in the same finite element. However, that does not take account of the interaction between fibres, such as crimp changes. In order to extend the approach to two fibre directions using rotation of the fibre, it is necessary to leave out the rotational derivatives that lead to orthotropic frames. A Lie derivative based on the deformation gradient **F** has been defined and implemented in ABAQUS. It is not exactly **F** that is used, but $\mathbf{F}_N$, which gives the same directions but keeps the unit vector with a norm equal to one. Examples of forming fabric simulations have been analysed in Hagège (2004). Figure 3.5 presents the different updates for the material axis and the associated objective derivatives described in this section.

3.3.2 Non-orthogonal constitutive models

In this method, the stress and strain of a continuous material are related to fibrous reinforcement using the constitutive relation in a non-orthogonal frame directed by the fibre directions. Models have been developed by Yu *et al.* (2002)

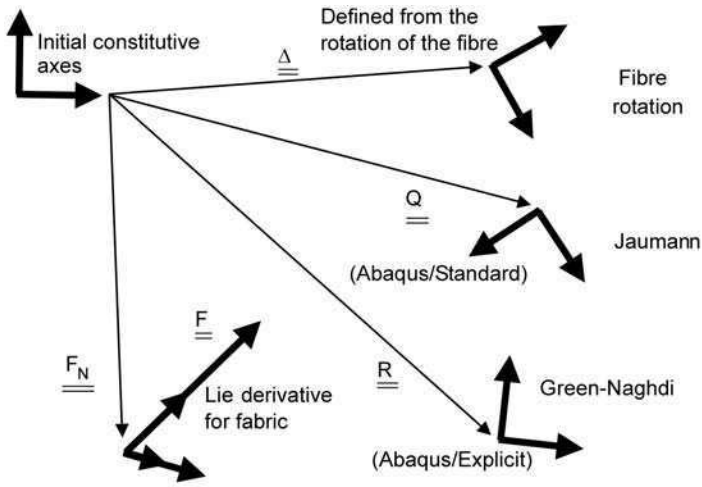

3.5 Material direction updates and objective derivatives (Hagège, 2004).

and Xue *et al.* (2003). They consider two yarn directions and use them to define the non-orthogonal frame. The second model, Xue *et al.* (2003) is briefly described here.

Figure 3.6 shows a local element of the continuum and the coordinates ξ and η along the warp and weft directions. x', y' are orthogonal coordinates with $x' = \xi$. The stress components in theses two frames can be related:

$$\begin{bmatrix} \sigma_{x'} \\ \sigma_{y'} \\ \sigma_{x'y'} \end{bmatrix} = \begin{bmatrix} 1 & 0 & 0 & 0 \\ 0 & 1 & -\cot\theta & -\cot\theta \\ -\cot\theta & \cot\theta & 0 & 1 \end{bmatrix} \begin{bmatrix} \sigma_\xi \\ \sigma_\eta \\ \tau_{\xi\eta} \\ \tau_{\eta\xi} \end{bmatrix} = T_2 \begin{bmatrix} \sigma_\xi \\ \sigma_\eta \\ \tau_{\xi\eta} \\ \tau_{\eta\xi} \end{bmatrix} \quad 3.13$$

$\tau_{\xi\eta}$ is not equal to $\tau_{\eta\xi}$ because ξ, η is non-orthogonal. The strains in the two frames are also related:

$$\begin{bmatrix} \epsilon_\xi \\ \epsilon_\eta \\ \gamma_{\xi\eta} \\ \gamma_{\eta\xi} \end{bmatrix} = \begin{bmatrix} 1 & 0 & 0 \\ \cos^2\theta & \sin^2\theta & \cos\theta\sin\theta \\ 0 & 0 & 1 \\ 0 & 0 & 1 \end{bmatrix} \begin{bmatrix} \epsilon_{x'} \\ \epsilon_{y'} \\ \epsilon_{x'y'} \end{bmatrix} = T_3 \begin{bmatrix} \epsilon_{x'} \\ \epsilon_{y'} \\ \epsilon_{x'y'} \end{bmatrix} \quad 3.14$$

ϵ_ξ and ϵ_η are the normal strains along warp and weft directions, $\gamma_{\xi\eta}$ and $\gamma_{\eta\xi}$ are the angular changes from the initial right-angle position. It can be assumed that the biaxial tensile properties and in-plane shear properties are independent. It has been shown experimentally that the biaxial tensions are affected only weakly by in-plane shear (Buet-Gautier *et al.*, 2001). The relation between stress and strain components in the non-orthogonal coordinates can be supposed in the form:

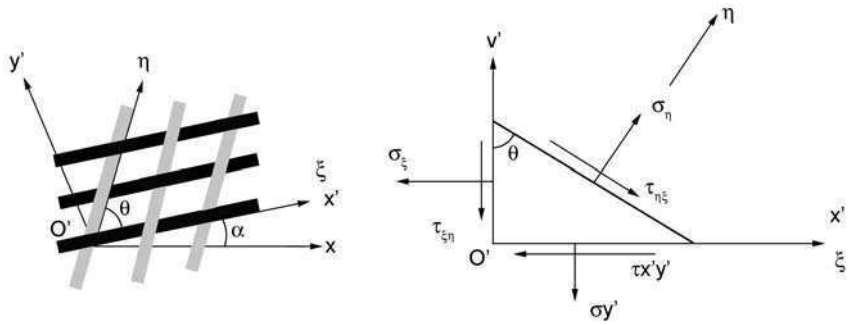

3.6 Orthogonal and non-orthogonal local frame and stress components on an isolated element (Xue *et al.,* 2003).

$$\begin{bmatrix} \sigma_\xi \\ \sigma_\eta \\ \tau_{\xi\eta} \\ \tau_{\eta\xi} \end{bmatrix} = \begin{bmatrix} D_{11} & D_{12} & 0 & 0 \\ D_{21} & D_{22} & 0 & 0 \\ 0 & 0 & \beta D_{33} & 0 \\ 0 & 0 & 0 & (2-\beta)D_{33} \end{bmatrix} \begin{bmatrix} \epsilon_\xi \\ \epsilon_\eta \\ \gamma_{\xi\eta} \\ \gamma_{\eta\xi} \end{bmatrix} = D \begin{bmatrix} \epsilon_\xi \\ \epsilon_\eta \\ \gamma_{\xi\eta} \\ \gamma_{\eta\xi} \end{bmatrix} \quad 3.15$$

$D_{11}, D_{22}, D_{12}, D_{21}$ are tension coefficients. D_{33} denotes the shear property. β is a coefficient that stands for contributions from each stress to shear. The constitutive equation can be expressed in the local orthogonal coordinates, and then in the global orthogonal coordinates.

$$[\boldsymbol{\sigma}]_{x'y'} = \mathbf{T}_2\mathbf{D}\mathbf{T}_3[\boldsymbol{\varepsilon}]_{x'y'} \qquad [\boldsymbol{\sigma}]_{xy} = \mathbf{R}\mathbf{T}_2\mathbf{D}\mathbf{T}_3\mathbf{R}^T[\boldsymbol{\varepsilon}]_{xy} \quad 3.16$$

R is the rotation matrix (3×3) that gives the components of an in-plane second order tensor in x, y from its components in x', y'. Equation (3.16) is a constitutive relation in the global frame using the properties in the fibre directions. The components D_{ij} of (3.15) can be identified from biaxial tests and in-plane shear tests (Xue *et al.*, 2003).

3.3.3 A macro-mechanical model used in a commercial FE code

The initial research and development work presented in this section was undertaken within a European Brite Euram project (BE 5092). Developments made under ESI PAM-STAMP led to the commercial FE code PAM-FORM, dedicated to composite forming and especially to reinforced thermoplastics (De Luca *et al.*, 1998; Pickett *et al.*, 2005).

An important point, frequently present in composite forming simulations, concerns the interface between plies. Several plies are often shaped together, especially in the case of reinforced thermoplastic composites. Each ply is kept discrete using shell elements. The friction loads are the summation of dry friction and viscous friction, see Fig. 3.7 (Pickett *et al.*, 2005).

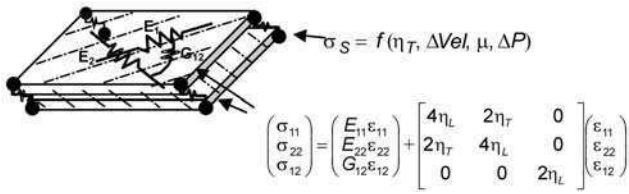

3.7 Two stacked plies and the constitutive laws for composite sheet forming (Pickett *et al.,* 2005).

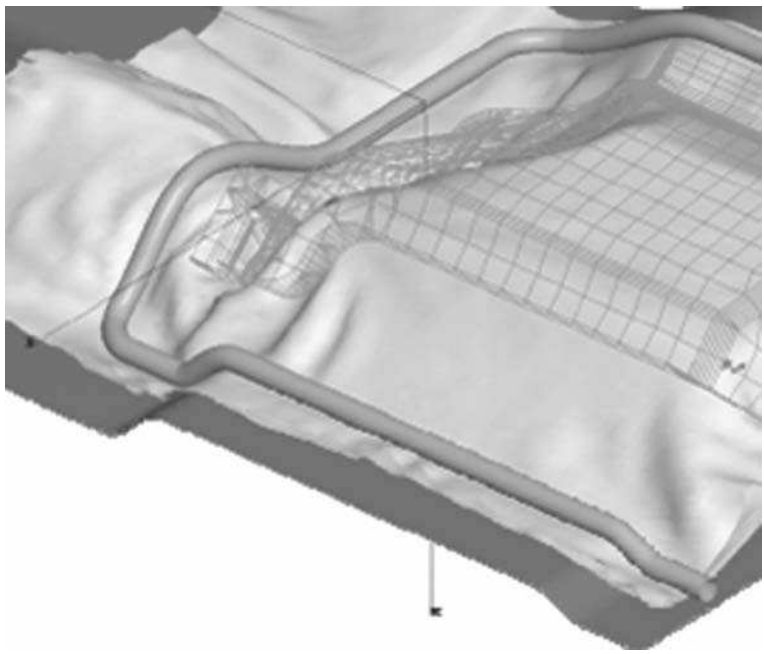

3.8 Simulation of the forming of a non-crimp fabric on the floor pan of a car (PAM-FORM ESI Group).

The mechanical behaviour of the ply is likened to elastic fibres embedded in a viscous resin (Ó Brádaigh *et al.*, 1993). Both resin longitudinal viscosity η_L and transverse viscosity η_T can be included. For dry fabrics, viscosity is ignored. The model can also be extended to NCF by modelling the stitching using spring elements (Pickett *et al.*, 2005). The simulation of the forming of a non-crimp fabric on the floor pan of a car is presented in Fig. 3.8, conducted by the ESI-Group using PAM-FORM within the European project TECABS.

3.4 Discrete or mesoscopic approach

The discrete approach is the opposite of the continuous approach, and considers and models the components of fibrous reinforcement at low scale. These

components can be yarns, woven cells or stitching, and also sometimes fibres. Because these elements are usually at the mesoscale (as defined in Section 3.2.1), the approach is also known as meso-mechanical modelling. Some analyses have been proposed where all fibres are modelled (microscale modelling) (Durville, 2002; Duhovic *et al.*, 2006; Pickett, 2002), but the number of fibres in a composite structure limits these computations to small sub-domains, for instance a woven cell or a few braided or knitted loops. Work in the field of discrete or mesoscopic analyses includes studies by Ben Boubaker *et al.* (2002, 2005), Cherouat *et al.* (2001), Ramgulam *et al.* (2005) and Pickett *et al.* (2005). A major difficulty lies in the description of the components at meso-scopic scale, usually the woven yarns. A compromise must be found between a precise description (which will be expensive from the computation time point of view) and a simple description, where it is possible to compute the entire forming process.

Beam and truss element are the more common descriptions for yarns (Cherouat *et al.*, 2001; Sharma *et al.*, 2003; Skordos *et al.*, 2005). Figure 3.9 shows the unit cell of a material made of four two-node trusses that represent the tows, and one (or two) truss elements to model shear stiffness (Sharma *et al.*, 2003). This approach has been used to simulate hemispherical draping (Skordos *et al.*, 2005).

Masses and springs are used to model the woven reinforcement in Fig. 3.10 (Ben Boubaker *et al.*, 2005). Springs are used to describe stretching, shear, bending and also elastic foundations. Drape deformation of a square fabric on a square surface has been performed using this model. The same authors seek to account for the crimp variations and yarn interaction, but the model is restricted to a plane cross-section and concerns a small number of woven cells.

Based on the above descriptions, a parallel can be drawn between fabric FE analysis and truss or beam structures such as those in civil engineering. Beam or truss elements can be used for FE analysis, but equivalent continuous models

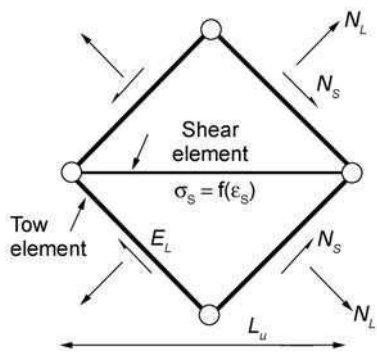

3.9 Unit cell made of four trusses for tows and one truss for shear stiffness (Sharma *et al.,* 2003).

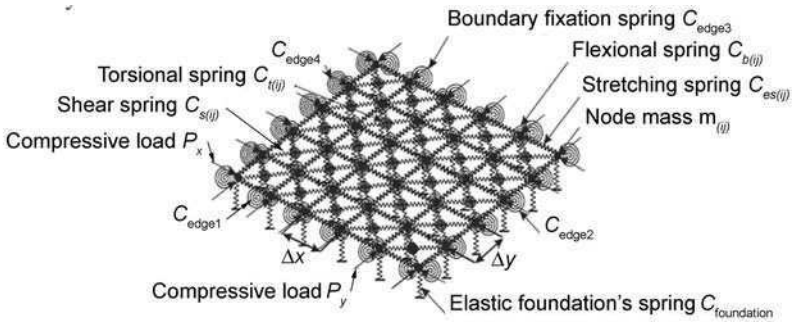

3.10 Discrete fabric model based on masses and springs (Ben Boubaker *et al.,* 2005).

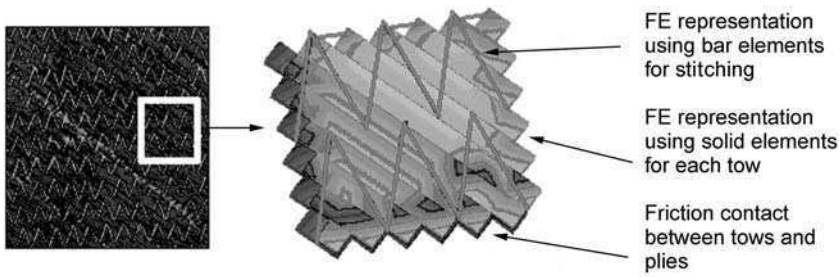

3.11 A 'representative cell' of the meso-mechanical model for NCF (Pickett *et al.,* 2005).

have been defined in order to compute structures with very large numbers of periodic beam patterns (Tollenaere *et al.*, 1998). Nevertheless, the complexity of the behaviour of a woven reinforcement cell is greater than that of a lattice cell.

In Pickett *et al.* (2005), meso-mechanical FE modelling of NCF uses 3D elements for each yarn and bar element for stitching (Fig. 3.11). Friction contact between tows and plies is taken into account. Although the complete model probably needs extensive computational time, a forming process has been simulated in this way (Pickett, 2005).

A point in favour of analysis at the mesoscopic scale lies in the strong increase in computer efficiency. Some discrete models that only work on small fabric parts will probably be used on a whole forming process in the near future.

3.5 Semi-discrete approach

The semi-discrete approach associates the FE method and a mesoscopic analysis of the woven unit cell. Specific finite elements are defined that are made of a discrete number of woven unit cells. The description of the fabric by finite

elements assumes that two points of weft and warp yarns initially superimposed remain superimposed after forming, i.e. there is no sliding between the yarns. This has been experimentally shown in most forming cases, as shown in Section 3.2.3 (Fig. 3.1).

3.5.1 Simplified dynamic equation for fabrics

Fabrics classically used as textile composite reinforcements have yarns made of thousands of small fibres, such as glass, carbon or aramid (Fig. 3.12a, b). Warp and weft yarns are woven following classical weaves, plain, satin or twill (Fig. 3.12c). This constitution leads to a fabric with very specific mechanical behaviour. Most of the rigidities are small or very small in comparison to tensile stiffness in the yarn directions. The mechanical behaviour of the unit woven cell for the model must be kept as simple as possible, i.e. must only account for significant mechanical quantities. The model will have to describe the specificities of textile reinforcement mechanical behaviour, especially:

- the non-linear tensile behaviour due to crimp interchange; and
- shear locking and the very different in-plane shear behaviour before and after this locking angle.

The diameter of the glass, carbon or aramid fibres is very small (a few μm) with regard to length. Consequently, the fibres can only be submitted to tension in their longitudinal direction $\mathbf{h}_1$ (Fig. 3.12a). The yarns usually used for composite reinforcements are composed of juxtaposed fibres in the same direction $\mathbf{h}_1$ (roving). Because relative sliding of the fibres is possible, the Cauchy stress state in the yarn, as well as in the fibres, is in the form (Fig. 3.12a,b):

$$\boldsymbol{\sigma} = \sigma^{11}\, \mathbf{h}_1 \otimes \mathbf{h}_1 \tag{3.17}$$

The tension in the yarn can be defined as:

$$T^{11} = \int_A \sigma^{11}\, \mathrm{d}S \qquad \mathbf{T} = T^{11}\, \mathbf{h}_1 \otimes \mathbf{h}_1 \tag{3.18}$$

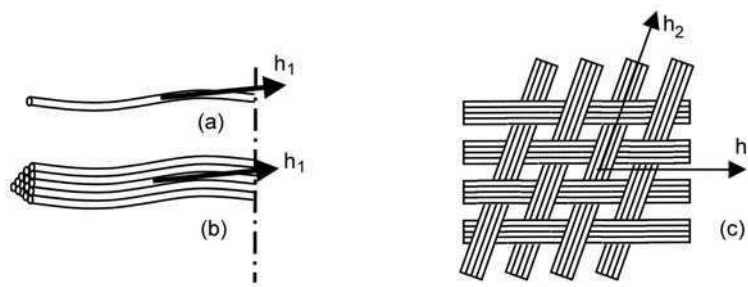

3.12 (a) Single fibre, (b) yarn made of juxtaposed fibres, (c) woven yarns.

A is the section of the yarn. This tension is a better defined quantity than the stress and is easier to measure. If a woven domain is considered (Fig. 3.12c), the tension tensor is in the form:

$$\mathbf{T} = T^{11}\,\mathbf{h}_1 \otimes \mathbf{h}_1 + T^{22}\,\mathbf{h}_2 \otimes \mathbf{h}_2 \tag{3.19}$$

where $\mathbf{h}_1$ and $\mathbf{h}_2$ are the vectors in warp and weft directions. In order to account for warp-weft interactions due to in-plane shear, i.e. warp-weft angle variations, a couple C, normal to the fabric, is considered at each crossover, or set of crossovers in the case of a more complex woven unit cell. Consequently, the global simplified dynamic equation is:

$$\sum_{p=1}^{\text{ncell}} \left({}^{p}\epsilon_{11}(\boldsymbol{\eta})\,{}^{p}T^{11}L_1 + {}^{p}\epsilon_{22}(\boldsymbol{\eta})\,{}^{p}T^{22}L_2\right) + \sum_{p=1}^{\text{ncell}} ({}^{p}C\;{}^{p}\gamma(\boldsymbol{\eta}) - W_{\text{ext}}(\boldsymbol{\eta}) = \int_{\Omega} \rho\;\ddot{\mathbf{u}} \cdot \boldsymbol{\eta}\;\mathrm{d}V \tag{3.20}$$

where $\boldsymbol{\varepsilon}(\boldsymbol{\eta}) = \nabla^{s}\boldsymbol{\eta} = \epsilon_{\alpha\beta}(\boldsymbol{\eta})\mathbf{h}^{\alpha} \otimes \mathbf{h}^{\beta}$ is the symmetrical gradient in the virtual displacement $\boldsymbol{\eta}$ (α and β are indexes taking value 1 or 2). $\mathbf{h}^1$, $\mathbf{h}^2$ are the contravariant vectors related to $\mathbf{h}_1$, $\mathbf{h}_2$, i.e. $\mathbf{h}_{\alpha} \cdot \mathbf{h}^{\beta} = \delta_{\alpha}{}^{\beta}$. L_1 and L_2 are the lengths of the warp and weft yarns in the midplane of the fabric. $\gamma(\boldsymbol{\eta})$ is the virtual relative rotation between warp and weft fibres (or virtual shear angle). ncell is the number of woven unit cells of the textile structure, ${}^{p}Q$, which means that the quantity Q is considered for the woven unit cell number p. $\ddot{\mathbf{u}}$ is the acceleration, ρ is the mass per volume of the fabric Ω. $W_{\text{ext}}(\boldsymbol{\eta})$ is the virtual work of the exterior prescribed loads.

To make an FE simulation of composite woven reinforcement forming based on the above approach, it is necessary to be able to calculate the tensions T^{11} and T^{22} and the shear couple C for a given strain field in the woven unit cell. It is assumed that the tension does not depend on the shear angle and that the shear couple does not depend on the axial strain, i.e. $T^{11}(\epsilon_{11}, \epsilon_{22})$, $T^{22}(\epsilon_{11}, \epsilon_{22})$ and $\mathrm{C}(\gamma)$. In Buet-Gauthier *et al.* (2001), biaxial tensile tests performed for different angles between warp and weft yarns showed that the influence of this angle is small and can be neglected. The second assumption (C only depending on γ) is probably less true (Dumont, 2003; Lomov *et al.*, 2004), nevertheless, all the currently available experimental results give the shear load as a function of the shear angle without any information on the tensions, so the assumption $\mathrm{C}(\gamma)$ will be made by default. Bending stiffness is not taken into account. For single- or few-layer textiles obtained by weaving yarns made of very small glass or carbon fibres and used as composite reinforcements, this is a justified assumption in most fabric forming processes.

3.5.2 Experimental and virtual test for tensile and in-plane shear behaviour

The weak form (3.20) requires knowledge of the two 'tension surfaces' $T^{11}(\epsilon_{11}, \epsilon_{22})$ and $T^{22}(\epsilon_{11}, \epsilon_{22})$. These surfaces can be obtained from a biaxial tensile test. Due to the weaving, the biaxial behavior of a fabric is complex and generally non-linear. Some experiments have been described in Kawabatta *et al.* (1973) and Buet-Gauthier *et al.* (2001). Biaxial tensile strains are prescribed to a cross-shaped woven specimen (Fig. 3.13) with different strain ratios (denoted k) in warp and weft directions. The tension measurements give the curve tensions as a function of axial strain for different warp-weft ratios. From this set of curves, the surface $T^{\alpha\alpha}(\epsilon_{11}, \epsilon_{22})$ for the given fabric can be extrapolated (Fig. 3.14). The tensile surfaces can also be obtained from three-dimensional FE computations on a unit cell as shown in Fig. 3.14 (Gasser *et al.*, 2000; Boisse *et al.*, 2001). These analyses are not classical, as the yarn is made of thousands of fibres and the mechanical behaviour of this assembly is very specific. The objective derivative based on the fibre rotation, as described in Section 3.3.1, must be used in order to follow the fibre direction exactly (Hagège *et al.*, 2005).

As shown in equation (3.17), a single fibre, and consequently an isolated yarn, can only be submitted to a tensile stress along its direction. When the yarns are woven, the interactions between warp and weft can create other stresses in the fabric. In-plane shear rigidity is of particular interest. It is very weak in most cases and sometimes insignificant in comparison with tension stiffness (Boisse *et al.*, 2001). The in-plane shear behaviour of fabric has been studied extensively, probably because it is the main deformation mode of fabrics (McGuinness *et al.*, 1997, 1998; Prodomou *et al.*, 1997; McBride *et al.*, 1997; Cao *et al.*, 2004).

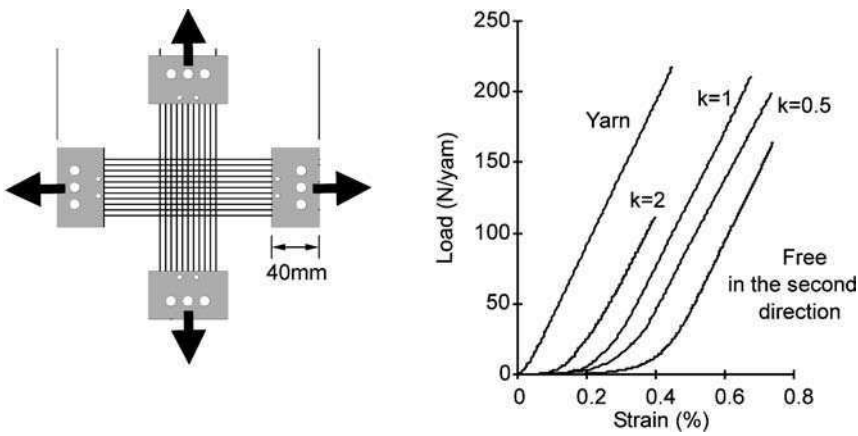

3.13 Cross shape specimen and tensile curves for different warp weft strain ratios k.

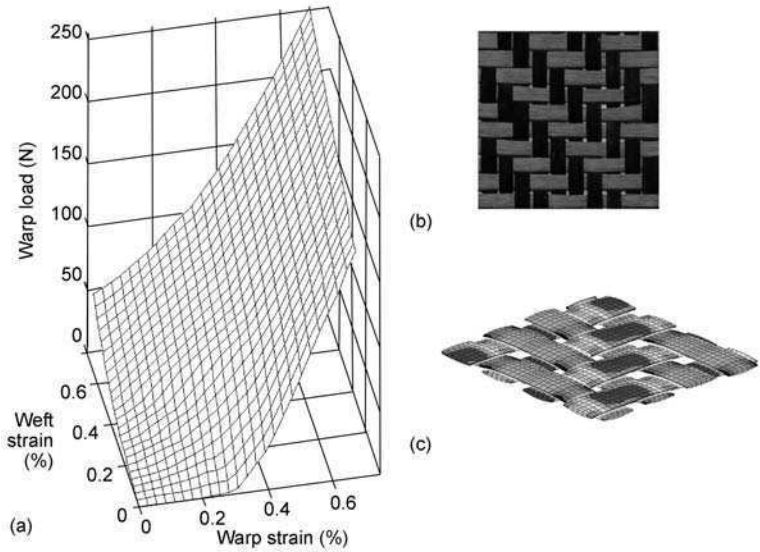

3.14 Tensile surface for a 2 × 2 twill of carbon.

The experimental in-plane shear behaviour of woven reinforcements can be analysed using a classical picture frame device (Fig. 3.15). Optical strain measurements can be taken at the macroscopic (pictures of the whole specimen), mesoscopic (a few woven cells) and microscopic levels within a yarn (Dumont, 2003). They permit both strain measures independent of the device and help us to understand the internal behaviour of the fabric during shearing. The strain fields are computed using an image correlation method (Raffel *et al.*, 1998; Vacher *et al.*, 1999). The macroscopic measures give the shear field versus the load on the picture frame and allow the homogeneity of the shear in the specimen to be checked. Figure 3.16 shows the load on the picture frame versus the shear strain in the case of a glass plain weave. In zone 1, the load is weak and the displacement field within the yarn (microscopic scale) shows that the yarn is submitted to rotation without local strain. The global shear of the fabric is entirely due to the relative motions of the yarns. The beginning of zone 2 corresponds to the shear-limit angle or shear-locking angle. The yarns start to be in contact with their neighbour and are laterally compressed, partially (zone 2), then totally (zone 3).

For a given shear angle γ the couple C can be deduced from the tension load on the picture frame. The power provided by the tension machine is assumed to be equally distributed on all woven unit cells.

$$\text{ncell } \mathrm{C}(\gamma) = \mathrm{F}(\gamma)V$$

and consequently

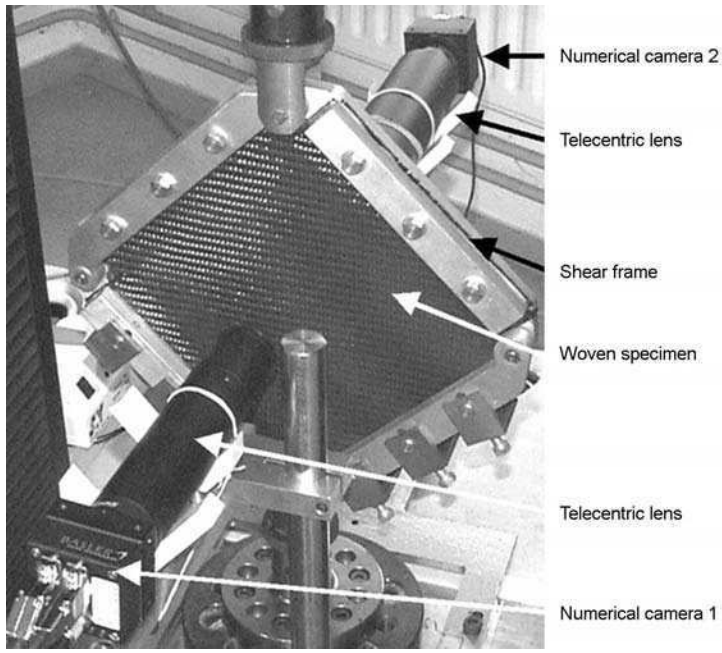

3.15 Shear frame device equipped with an optical system.

$$C(\gamma) = \frac{a}{\text{ncell}} \frac{\sqrt{2}}{2} \left(\cos \frac{\gamma}{2} - \sin \frac{\gamma}{2} \right) F(\gamma) \qquad 3.21$$

where a is the length of the side of the frame (between two pin-joints), F is the load on the tension machine for a shear angle γ and V is the speed of the tension machine.

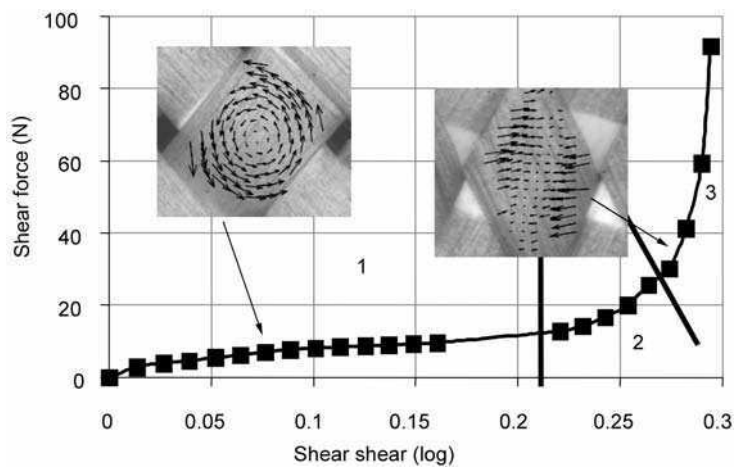

3.16 Shear curve and optical analysis (Dumont, 2003).

This shear curve can also be obtained from three-dimensional FE analysis on a unit cell submitted to in-plane shear (Boisse *et al.*, 2005b), although this analysis is difficult due to the contact localisation beyond the shear-locking angle.

3.5.3 A four-node finite element made of woven cells

From our knowledge of the tension surfaces ($T^{11}(\epsilon_{11}, \epsilon_{22})$ and $T^{11}(\epsilon_{11}, \epsilon_{22})$) and of the shear curve (C(γ)), the simplified dynamic equation (3.5) permits us to construct specific finite elements for fabric forming (Boisse *et al.*, 2005a; Zouari *et al.*, 2006).

The four-node element is presented in Fig. 3.17. It is made of ncell^e woven cells. The directions of the yarns are those of the natural coordinates in the reference element ξ_1, ξ_2, i.e. the directions of the sides of the element. There are two main reasons for this. First, the numerical efficiency is improved because the expressions of the interior load components are much simpler. Secondly, it has been shown that, in the case of a material with two directions that are very stiff in comparison with others (especially woven materials), the finite element analyses can lead to locking if these directions are not those of the element sides (Yu *et al.*, 2004).

Because the computations are made using an explicit approach, the only quantity needed is the elementary interior nodal load $\mathbf{F}^e_{int}$ that is related to the interior elementary work W^e_{int}:

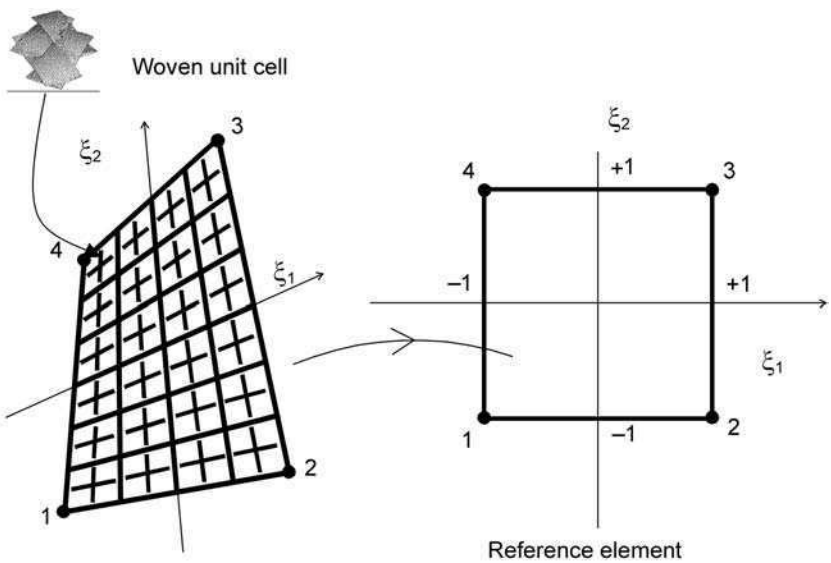

3.17 Four node finite element made of woven cells.

$$W_{\text{int}}^{\text{e}}(\boldsymbol{\eta}) = \sum_{p=1}^{\text{ncell}^{\text{e}}} ({}^{p}\epsilon_{11}(\boldsymbol{\eta})\ {}^{p}T^{11}\,{}^{p}L_1) + {}^{p}\epsilon_{22}(\boldsymbol{\eta})\,{}^{p}T^{22}\,{}^{p}L_2 + \sum_{p=1}^{\text{ncell}^{\text{e}}} {}^{p}\gamma(\boldsymbol{\eta})^{p}\text{C}$$
$$= \eta_s(\text{F}_{\text{int}}^{\text{e}})_s \tag{3.22}$$

The nodal index s varies from 1 to 12 in the case of the four-node quadrilateral.

The symmetrical gradient of the virtual displacement is expressed in $\mathbf{h}^1$, $\mathbf{h}^2$ and $\mathbf{g}^1$, $\mathbf{g}^2$:

$$\nabla^s\boldsymbol{\eta} \ = \epsilon_{\alpha\beta}\mathbf{h}^\alpha \otimes \mathbf{h}^\beta = \bar{\epsilon}_{\alpha\beta}\mathbf{g}^\alpha \otimes \mathbf{g}^\beta \tag{3.23}$$

$\mathbf{g}_1$, $\mathbf{g}_2$ is the covariant material base such as $\mathbf{g}_\alpha = \partial x/\partial\xi_\alpha$ and $\mathbf{g}^\alpha$ the related contravariant vectors.

The strain interpolation components $B_{\alpha\alpha s}$ are defined from the virtual strain components $\bar{\epsilon}_{\alpha\alpha}$:

$$\bar{\epsilon}_{\alpha\alpha} = \frac{\partial\boldsymbol{\eta}}{\partial\xi_\alpha}\cdot\mathbf{g}_\alpha = \frac{\partial N^k}{\partial\xi_\alpha}(\mathbf{g}_\alpha)_m\eta_s = B_{\alpha\alpha s}\eta_s \tag{3.24}$$

where k = integer part of $(s+2)/3$ and $m = s - 3(k-1)$. To define the interpolation of the angle ${}^{p}\gamma(\boldsymbol{\eta})$, a first order development is required. The rotation between warp and weft yarns corresponding to the virtual displacement η is:

$$\gamma(\boldsymbol{\eta}) = \arccos\left(\frac{\mathbf{g}_{1\eta}\cdot\mathbf{g}_{2\eta}}{\|\mathbf{g}_{1\eta}\|\,\|\mathbf{g}_{2\eta}\|}\right) - \arccos\left(\frac{\mathbf{g}_1\cdot\mathbf{g}_2}{\|\mathbf{g}_1\|\,\|\mathbf{g}_2\|}\right) \tag{3.25}$$

where $\mathbf{g}_\alpha = \partial\mathbf{x}/\partial\xi_\alpha$ and $\mathbf{g}_{\alpha\eta} = [\partial(\mathbf{x}+\boldsymbol{\eta})]/\partial\xi_\alpha$ are the material covariant vectors respectively in the current and virtual configuration.

Denoting $\theta = (\mathbf{g}_1, \mathbf{g}_2)$ and $\theta_\eta = (\mathbf{g}_{1\eta}, \mathbf{g}_{2\eta}) = \theta + \gamma(\boldsymbol{\eta})$ and neglecting the second order terms, equation (3.12) can be approximated by:

$$\gamma(\boldsymbol{\eta}) = \frac{\partial\boldsymbol{\eta}}{\partial\xi_1}\cdot\left[\operatorname{cotg}\theta\frac{\mathbf{g}_1}{\|\mathbf{g}_1\|^2} - \frac{\mathbf{g}_2}{\sin\theta\,\|\mathbf{g}_1\|\,\|\mathbf{g}_2\|}\right]$$
$$+ \frac{\partial\boldsymbol{\eta}}{\partial\xi_2}\cdot\left[\operatorname{cotg}\theta\frac{\mathbf{g}_2}{\|\mathbf{g}_2\|^2} - \frac{\mathbf{g}_1}{\sin\theta\,\|\mathbf{g}_1\|\,\|\mathbf{g}_2\|}\right] \tag{3.26}$$

This gives the shear strain interpolation:

$$\gamma(\boldsymbol{\eta}) = B_{\gamma s}\eta_s \tag{3.27}$$

With:

$$B_{\gamma s} = \frac{\partial N^k}{\partial\xi_1}\left[\operatorname{cotg}\theta\frac{(g_1)_m}{\|\mathbf{g}_1\|^2} - \frac{(g_2)_m}{\sin\theta\|\mathbf{g}_1\|\,\|\mathbf{g}_2\|}\right]$$
$$+ \frac{\partial N^k}{\partial\xi_2}\left[\operatorname{cotg}\theta\frac{(g_2)_m}{\|\mathbf{g}_2\|^2} - \frac{(g_1)_m}{\sin\theta\|\mathbf{g}_1\|\,\|\mathbf{g}_2\|}\right] \tag{3.28}$$

From the strain interpolation coefficients $B_{\alpha\alpha s}$ and $B_{\gamma s}$ obtained in (3.11) and (3.15), the virtual elementary interior load work is related to virtual displacements:

$$W_{\text{int}}^{\text{e}}(\boldsymbol{\eta}) = \eta_s \left(\sum_{p=1}^{\text{ncell}^{\text{e}}} \|\mathbf{g}_1\|^{-2} \, {}^{p}B_{11s} \, {}^{p}T^{11} + \|\mathbf{g}_2\|^{-2} \, {}^{p}B_{22s} \, {}^{p}T^{22} + {}^{p}C \, {}^{p}B_{\gamma s} \right)$$
$$= \eta_s (\mathbf{F}_{\text{int}}^{\text{e}})_s \qquad 3.29$$

As shown in Boisse (1994), computation of the nodal interior loads does not require the summation on all the woven cells of the element. Accounting for the bilinear interpolation, the summation can be done on only four cross-overs, the positions of which depend on the number of warp and weft yarns. If n_c and n_t are the number of yarns in warp and weft directions, the position of the four cross-overs are:

$$\lambda_1 = (-1)^{\gamma} \left((n_c^2 - 1)(3n_c^2)^{-1} \right)^{1/2} \quad \lambda_2 = (-1)^{\delta} \left((n_t^2 - 1)(3n_t^2)^{-1} \right)^{1/2} \qquad 3.30$$

and δ are equal to 1 or 2. Consequently, the nodal interior load components can be calculated by:

$$(\mathrm{F}_{\text{int}}^{\text{e}})_s = \sum_{\gamma=1}^{2} \sum_{\delta=1}^{2} \frac{n_c n_t}{4} \begin{pmatrix} B_{11s}(\lambda_1, \lambda_2) L_1 T^{11}(\lambda_1, \lambda_2) \|\mathbf{g}_1(\lambda_1, \lambda_2)\|^{-2} \\ + B_{22s}(\lambda_1, \lambda_2) L_2 T^{22}(\lambda_1, \lambda_2) \|\mathbf{g}_2(\lambda_1 . \lambda_2)\|^{-2} \\ + B_{\gamma s}(\lambda_1, \lambda_2) \mathrm{C}(\lambda_1, \lambda_2) \end{pmatrix} \qquad 3.31$$

This expression is explicit, there is no matrix multiplication, no computation of terms equal to zero (corresponding for instance to non-existent stiffness in fabrics). Consequently, the numerical efficiency of the element is good.

3.5.4 Hemispherical forming of an unbalanced fabric

The hemispherical forming of a 2×2 nylon twill is analysed in this section. This type of fabric is used in the automotive industry (Dumont, 2003). It exhibits a very unbalanced tensile behaviour in warp and weft directions (Fig. 3.18). The shear behaviour of this fabric has been analysed experimentally using the picture frame test. Its rigidity has been investigated using two straight segments, whose slopes are $k_1 = 0.03$ mmN/rd and $k_2 = 0.095$ mmN/rd with a critical shear angle $\gamma_c = 0.5$rd. Tests of hemispheric sheet-forming have been carried out by F. Dumont in the S3MEM composites laboratory of the University of Nottingham (Daniel *et al.*, 2003). The forming process was simulated using two approaches, tension only, and tension plus shear. The results of these two simulations as well as the experimental final shape are shown in Fig. 3.19. The experimental deformed shape is very different in warp and weft directions. The warp direction (vertical in Fig. 3.19 and corresponding to the most rigid yarns), shows significant sliding of fabric in the matrix. In the weft direction, there is no visible

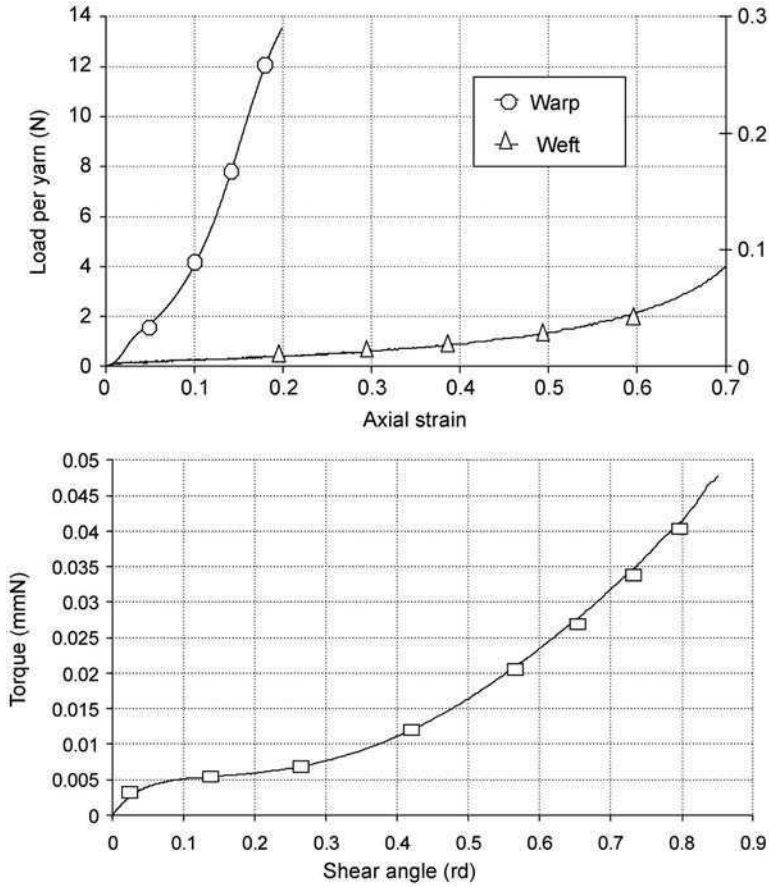

3.18 Characteristics of the woven reinforcement, in tension (warp and weft direction), and in shear.

sliding. The yarns are strongly stretched. At the summit of the hemisphere, an initially square quadrilateral becomes a rectangle with a side ratio equal to 1.8 (Fig. 3.19a). Both simulations give a value of this ratio close to the experimental value (Figs 3.19b and 3.19c). The deformation of the hemispherical part is computed well by both approaches.

The asymmetry of the deformed shape in warp and weft directions is obtained by both approaches. The main difference concerns the wrinkles. In the tension plus shear approach, the shear strain energy leads to the appearance of wrinkles in the plane region of the preform, whereas for tension only, there are no wrinkles. The shapes are in good agreement with those of the experimental preform (Figs 3.19a and 3.19c). There are no wrinkles in the hemispherical zone and the two approaches give close results in this region. But there are regions where the shear angle is higher than the shear-limit angle. When the shear

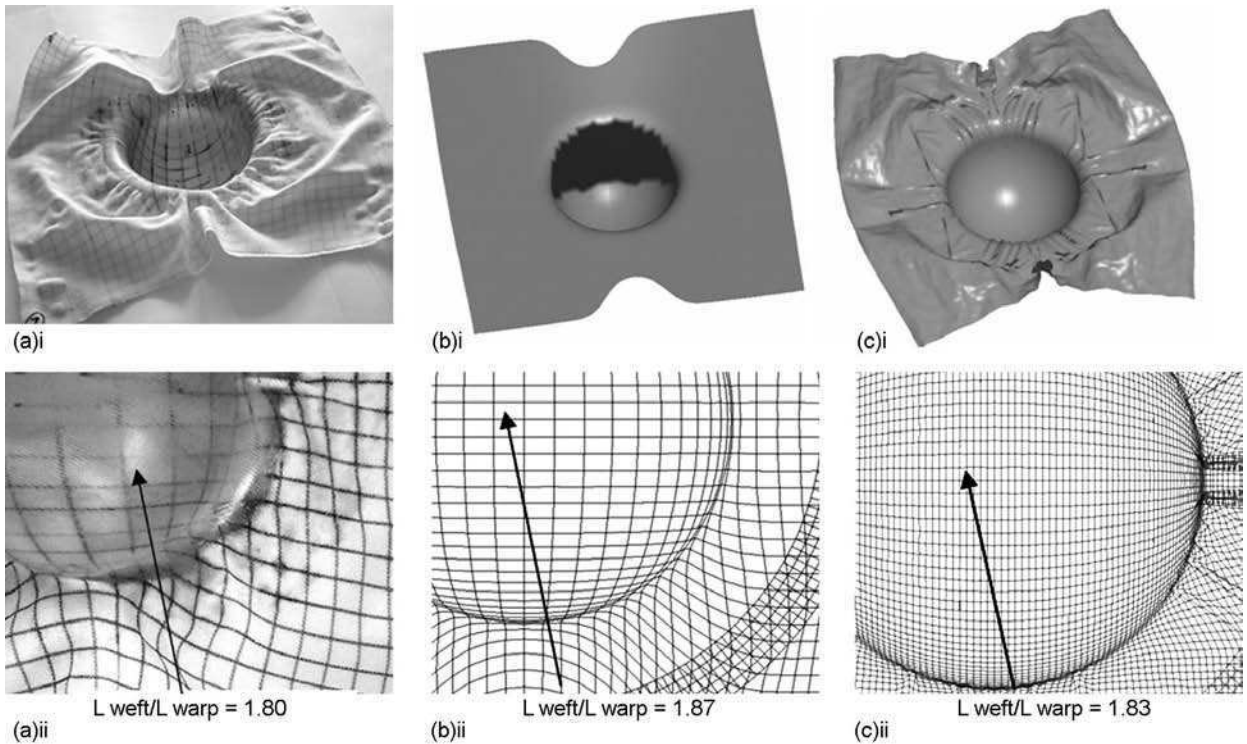

3.19 Deformed shape after the hemispheric forming in the experimental case (a), simulation in tension only (b) and in tension plus shear (c).

energy is taken into account, the minimisation of the total deformation energy leads to an out-of-plane solution, i.e. the wrinkles (Fig. 3.19c). The contribution of shear behaviour is mainly in describing the state after the appearance of wrinkles. At this stage, the relative rotations between warp and weft yarns are reduced. For instance, the maximum shear angle is 38º in Fig. 3.19c as opposed to 50º in Fig. 3.19b. This value (38º in the case of tension plus shear analysis) is in good agreement with angles measured experimentally (37º). It should be pointed out that the mesh used in Fig. 3.19c (tension plus shear) is finer than that used in Fig. 3.19b (tension only). These meshes can be used because their thickness does not change the solution significantly. The mesh size can be much finer in the case of tension plus shear because the wrinkles that appear in this case need much smaller elements in order to describe the wrinkles correctly, without using any perturbation methods or initial imperfections.

3.6 Multi-ply forming and re-consolidation simulations

There are several composite forming processes in which the transverse behaviour, i.e. the strain and stress across the thickness, is a major issue. That is the case for Continuous Fibres and ThermoPlastic (CFRTP) matrix forming processes (Maison *et al.*, 1998). After heating at a temperature higher than the melting point (Fig. 3.20a), forming is carried out using a punch and die process, normally using a rubber on the die (Fig. 3.20b). Re-consolidation is obtained by applying pressure on the punch (Fig. 3.20c). The objective of this last stage is to remove any residual pores at the interface of the plies, which is critical for products such as load-bearing aeronautical parts.

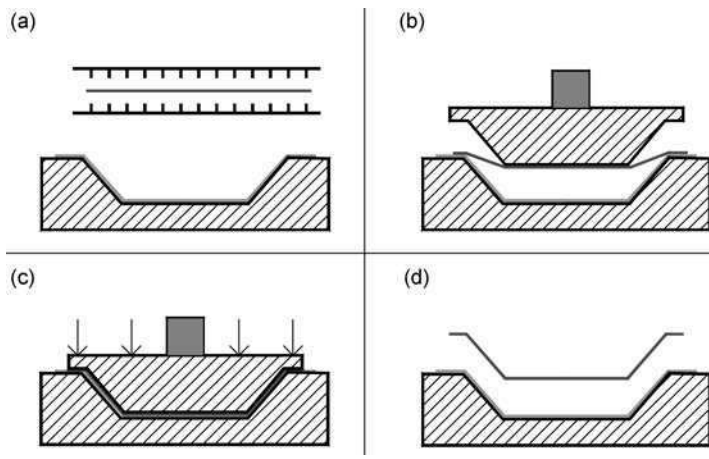

3.20 Different stages of forming. (a) Heating of the CFRTP. (b) Forming with punch and die. (c) Reconsolidation phase. (d) Final part.

3.6.1 Simulation of CFRTP forming processes

One of the main forming modes is the relative sliding between the plies. In order to permit the necessary sliding, each ply is modelled as a set of shell elements. An example is shown in Fig. 3.21 for a Z reinforcement made of ten plies that slide during bending of the initially flat plate. The relative sliding between the plies (Fig. 3.22) agrees with experimental results (Cheruet *et al.*, 2002).

An important quality issue for the final part is the absence of pores in the thickness of the composite. Any pores could be the source of a fracture during the service life of the composite and must be avoided, particularly for aeronautical applications. This is the reason behind the re-consolidation stage of the forming process (Fig. 3.20). It has been shown that many gaps appear in the material after the heating stage (Fig. 3.23) and these are removed by the pressure applied during the re-consolidation phase (Fig. 3.24). This stage is essential to

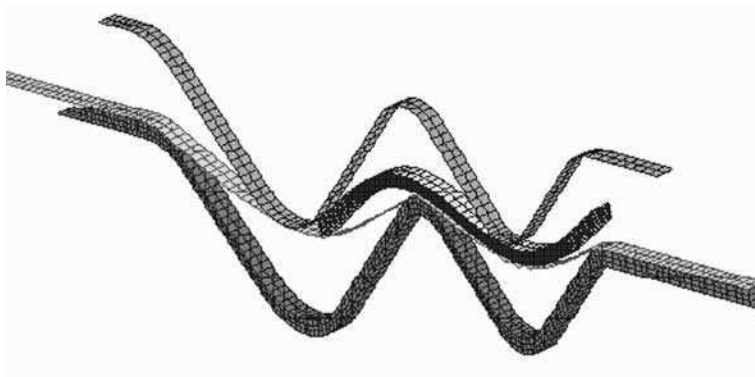

3.21 Forming of a Z reinforcement. Forming stage (Cheruet *et al.,* 2002).

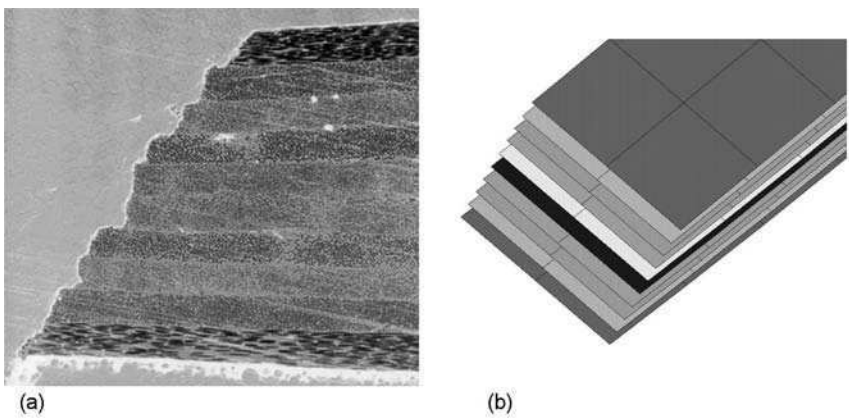

3.22 Interply sliding during the forming stage (Cheruet *et al.,* 2002).

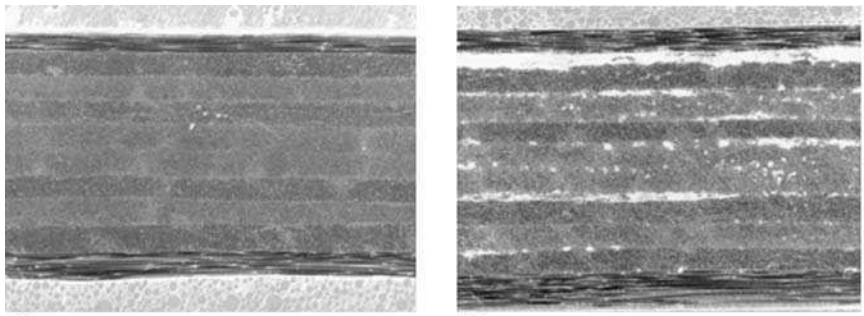

3.23 Material before and after the heating stage (Cheruet *et al.,* 2002).

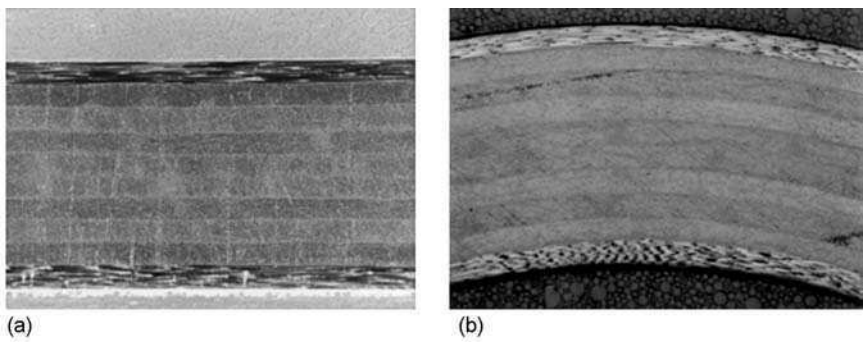

3.24 Material state after the re-consolidation stage (Cheruet *et al.,* 2002).

the final quality of the part. It can be analysed by an FE simulation to determine if the stress through the thickness is sufficient to remove any pores.

3.6.2 Shell element with pinching

Re-consolidation has been studied by Lee *et al.* (1987) and some models for local consolidation have been proposed. These studies have shown that re-consolidation depends on the stress state in the laminate, and mainly on the normal stress in the re-consolidation stage. This stress component is not present in classical shell theory. Some finite elements with stress/strain through the thickness have been proposed (Simo *et al.*, 1990; Butcher *et al.*, 1994; Bletzinger *et al.*, 2000). A shell element is used where a degree of freedom through the thickness strain is introduced (Coquery, 1999; Cheruet *et al.*, 2002). The thickness stress is not equal to zero but is related to the thickness variation β by the constitutive law. Assuming small rotations between two computation steps, the displacement expression is (Fig. 3.25):

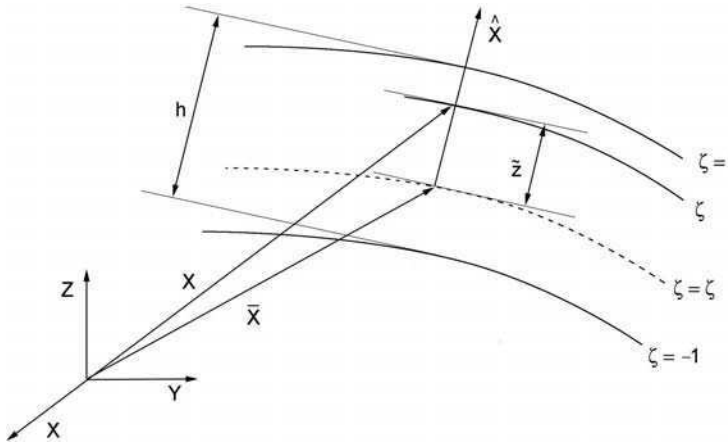

3.25 Kinematics of the shell with pinching.

$$u = \bar{u} - \tilde{z}^0 \hat{X}^t \times \theta + z\beta\hat{X}^t \tag{3.32}$$

If $\beta = 0$ then equation (3.32) leads to classical shell kinematics without pinching. β is a additional pinching degree of freedom. The strain tensor $\epsilon(\mathbf{u}) = \frac{1}{2}[\nabla(\mathbf{u}) + \nabla^T(\mathbf{u})]$ can be derived from to the displacement (3.9).

In an orthogonal frame $(\hat{\mathbf{e}}_1, \hat{\mathbf{e}}_2, \hat{\mathbf{e}}_3 = \hat{\mathbf{X}})$ the membrane bending strain components are:

$$\begin{Bmatrix} \epsilon_{11} \\ \epsilon_{22} \\ 2\epsilon_{12} \end{Bmatrix} = \begin{Bmatrix} u^m_{x,1} \\ u^m_{y,2} \\ u^m_{y,1} + u^m_{x,2} \end{Bmatrix} + z \begin{Bmatrix} \theta_{y,1} \\ -\theta_{x,2} \\ -\theta_{x,2} + \theta_{y,1} \end{Bmatrix} \tag{3.33}$$

The transverse shears are:

$$\begin{Bmatrix} 2\epsilon_{13} \\ 2\epsilon_{23} \end{Bmatrix} = \begin{Bmatrix} u^m_{z,1} + \theta_y \\ u^m_{z,2} - \theta_x \end{Bmatrix} + z \begin{Bmatrix} \beta_{,1} \\ \beta_{,2} \end{Bmatrix} \tag{3.34}$$

and the strain through the thickness (pinching) is:

$$\{\epsilon_{33}\} = \beta \tag{3.35}$$

The transverse shear strains are modified by pinching. In contrast to the classical shell, the normal stress through the thickness is not zero. It is deduced from $\epsilon_{33} = \beta$ using the compaction behavior law. It has been shown that this element exhibits a 'pinching' locking. To avoid this locking, it is necessary to modify the constitutive relation in order to remove the coupling between pinching and bending (Coquery, 1999; Cheruet *et al.*, 2002). The example presented in Fig. 3.26 (cantilever plate) shows the pinching locking obtained with a complete behaviour law and the accurate result if pinching and bending are not coupled. Analysis of the reason for this locking can be found in Soulat *et al.* (2006).

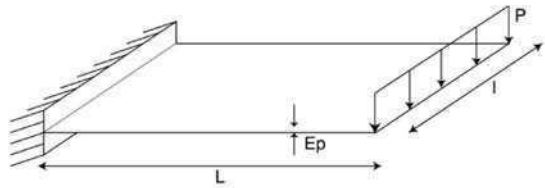

Transverse displacement (m)			
Thickness (m)	Traditional shell element	Shell with pinching element, including bending uncoupling	Shell with pinching element with 3D behaviour
0.01	-0.044	-0.044	-0.038
0.001	-0.044	-0.044	-0.037
0.0001	-0.044	-0.044	-0.031

3.26 Effectiveness of uncoupling bending-pinching.

3.6.3 Simulation of the forming and re-consolidation stage of a Z profile

Using the shell element described above, the stress through the thickness is computed for an initially flat ply which is formed into a Z shape (Fig. 3.21) and then compacted.

During and at the end of the forming stage (Fig. 3.27), the stress through the thickness is equal to zero in most areas except in the radius of the tools. That confirms micrographic observations which have shown that consolidation only occurs near the radius during the forming stage (Cheruet *et al.*, 2002).

After the compaction phase, the entire part is in compression (Fig. 3.28). The value of the stress through the thickness is related to the angle of the curved part of the Z profile. In order to obtain an accurate value of the thickness stress, it is important to used an efficient non-linear compaction law (Gutowski, 1985; Baoxing *et al.*, 1999).

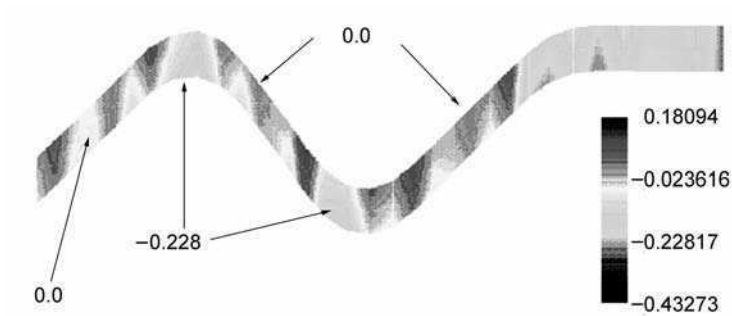

3.27 Stress component through the thickness at the end of forming.

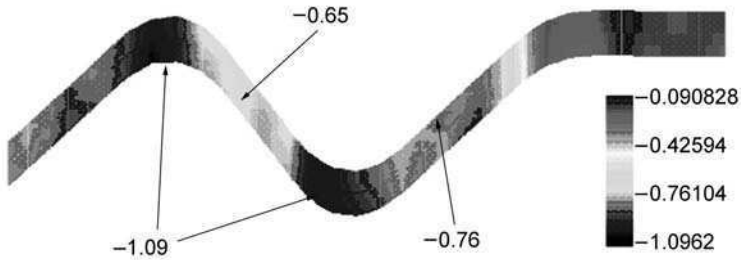

3.28 Stress component through the thickness after the re-consolidation stage.

3.7 Conclusions

Finite element analysis is probably the approach that will be used to simulate composite forming processes in the future. These simulations are especially important for composite materials because not only do they help determine the feasibility of the forming process itself, but they also give fibre directions and densities, which are essential for further analysis of the composite part in service. The deformation modes of the composite during forming are related mainly to the internal fibrous structure of the reinforcement, consequently the forming modes are specific to these materials. Fibre extensions are usually small, but large in-plane shear can occur.

At present, two approaches are used. The continuous approach involves defining an equivalent continuous mechanical behaviour for the fibrous reinforcement at the macroscopic level, and the discrete or mesoscopic approach models the components of the reinforcement at the mesoscopic level. While most industrial analysis currently uses the continuous approach, the mesoscopic approach will become more common as analysts take advantage of computing improvements.

One point must be underlined at the end of this chapter. It concerns the necessity for accurate tests (experimental or virtual) to determine the mechanical properties of the materials, including friction. The FE method is a mechanical approach and understanding the behaviour of the material during forming is essential for the computations. Tests for composite reinforcements are not as well established as those for metallic materials, for instance a cooperative benchmark performed by several labs on in-plane shear properties has shown a large variation in results for a glass fibre fabric used in automotive applications. This area must be improved if FE analysis for composite forming is to be accurate.

3.8 References

ABAQUS FEA software, www.abaqus.com
Argyris J (1960), *Energy Theorems and Structural Analysis*, Butterworths, London.

Baoxing C, Chou T W (1999), Compaction of woven-fabric preforms in liquid composite molding processes: single layer deformation, *Composite Science and Technology*, 59, 1519–1526.

Ben Boubaker B, Haussy B, Ganghoffer J F (2002), 'Discrete models of woven structures, draping and stability analysis', *CRAS Paris, Série Mécanique*, 330, 871–877.

Ben Boubaker B, Haussy B, Ganghoffer J F (2005), 'Discrete models of fabrics accounting for yarn interactions', *European Journal of Computational Mechanics*, 14 (6–7), 653–676.

Bletzinger K U, Bischoff M, Ramm E (2000), 'A unified approach for shear-locking free triangular shell finite elements', *Computer and Structures*, 75, 321–334.

Boisse P, (1994), *Modèles mécaniques et numériques pour l'analyse non-linéaire des structures minces*, Thesis for PhD direction enabling, University of Besançon, France.

Boisse P, Gasser A, Hivet G (2001), 'Analyses of fabric tensile behaviour: determination of the biaxial tension-strain surfaces and their use in forming simulations', *Composites A*, 32, 1395–1414.

Boisse P, Zouari B, Gasser A (2005a), 'A mesoscopic approach for the simulation of woven fibre composite forming', *Composites Science and Technology*, 65, 429–436.

Boisse P, Gasser A, Hagège B, Billoet J L (2005b), 'Analysis of the mechanical behaviour of woven fibrous material using virtual tests at the unit cell level', *Int. Journal of Material Science*, 40, 5955–5962.

Borouchaki H, Cherouat A (2003), 'Geometrical draping of composites', *Comptes Rendus de l'Académie des Sciences*, Paris, Série II B, 331, 437–442.

Bréard J, Saouab A (2005), 'Numerical simulation of liquid composite molding processes', *European Journal of Computational Mechanics*, 14 (6–7), 841–865.

Buet-Gautier K, Boisse P (2001), 'Experimental analysis and modeling of biaxial mechanical behavior of woven composite reinforcements', *Experimental Mechanics*, 41 (3), 260–269.

Butcher N, Ramm E, Roehl D (1994), 'Three dimensional extension of non-linear shell formulation based on the enhanced assumed strain concept'. *Int. J. for Num. In Engng*., 37, 2551–2568.

Cao J, Cheng H S, Yu T X, Zhu B, Tao X M, Lomov S V, Stoilova Tz, Verpoest I, Boisse P, Launay J, Hivet G, Liu L, Chen J, De Graaf E F, Akkerman R (2004), 'A cooperative benchmark effort on testing of woven composites', *Proceedings of the 7th Int. ESAFORM Conference on Material Forming*, Trondheim (Norway), 305–308.

Cherouat A, Billoët J L (2001), 'Mechanical and numerical modelling of composite manufacturing processes deep-drawing and laying-up of thin pre-impregnated woven fabrics', *J. Mat. Proc. Technology*, 118, 460–471.

Cheruet A, Soulat D, Boisse P, Soccard E, Maison-Le Poec S (2002), 'Analysis of the interply porosities in thermoplastic composites forming processes', *International Journal of Forming Processes*, 5, (2–4), 247–258.

Chinesta F, Cueto E, Ryckelynck D, Ammar A (2005), 'Numerical simulation of liquid composite molding processes', *European Journal of Computational Mechanics*, 14, (6–7), 903–923.

Comas-Cardona S, Groenenboom P H L, Binétruy C, Krawczak P (2005), 'Simulation of liquid composite molding processes using a generic mixed FE-SPH method', *European Journal of Computational Mechanics*, 14 (6–7), 867–883.

Coquery M H (1999), *Modélisation d'un joint de culasse multifeuille*, PhD Thesis, ENSAM Paris.

Criesfield M A (1991), *Non linear finite element analysis of solids and structures*, *II: Advanced topics*, John Wiley & Sons.

Dafalias Y F (1983), 'Corotational rates for kinematic hardening at large plastic deformations', *Trans. of the ASME, J. of Ap. Mech*., 50, 561–565.

Daniel J L, Soulat D, Dumont, F, Zouari B, Boisse P, Long A C (2003), 'Forming of a very unbalanced fabric. Experiment and simulation', *International Journal of Forming Processes*, 6 (3–4), 465–480.

Darcy H (1856), 'Les Fontaines Publiques de La Ville De Dijon: Distribution d'Eau et Filtrage Des Eaux'*, Appendice – Note D*, Victor Dalmont, Paris.

De Luca P, Pickett A K (1998), 'Numerical and experimental investigation of some press forming parameters of two fibre reinforced thermoplastics: APC2-AS4 and PEI-CETEX', *Composites Part A*, 29, 101–110.

Dienes J K (1979), 'On the analysis of rotation and stress rate in deforming bodies', *Acta Mechanica*, 32, 217–232.

Duhovic M, Bhattacharyya D (2006), 'Simulating the deformation mechanisms of knitted fabric composites', *Composites A,* 37 (11) 1897–1915.

Dumont F (2003). *Contribution à l'expérimentation et à la modélisation du comportement mécanique de renforts de composites tissés*, PhD Thesis, Université Paris 6.

Dumont P, Orgéas L, Corre S L, Favier D (2003), 'Anisotropic viscous behavior of sheet molding compounds (SMC) during compression molding', *Int . J. Plasticity*, 19, 625–646.

Durville D (2002), 'Modélisation par éléments finis des propriétés mécaniques de structures textiles: de la fibre au tissu', *European Journal of Computational Mechanics*, 11 (2–4), 463–477.

ESI-QuickFORM, PAM-FORM, PAM-STAMP, *www.esi-groupe.com*

FiberSIM, www.vistagy.com

Fournier R, Coupez T, Vincent M (2005), 'Numerical determination of the permeability of fibre reinforcement for the RTM process', *European Journal of Computational Mechanics*, 14 (6–7), 803–818.

Gasser A, Boisse P, Hanklar S (2000), 'Analysis of the mechanical behaviour of dry fabric reinforcements. 3D simulations versus biaxial tests'. *Computational Material Science*, 17, 7–20.

Gilormini P, Roudier P, Rougee P (1993), 'Cumulated tensorial deformation measures', *Comptes-rendus de l'Académie des Sciences de Paris* II, 316, 1499–1504.

Gingold R A, Monaghan J J (1977), 'Smoothed particle hydrodynamics: Theory and application to non-spherical stars', *Mon. Not. R. Astr. Soc*., 181, 375–389.

Gutowski T G (1985), 'A resin flow/fibre deformation model for composites'*, SAMPE Quart*, 16 (4), 58–64.

Hagège B (2004), *Simulation du comportement mécanique des milieux fibreux en grandes transformations: application aux renforts tricotés*, PhD Thesis, ENSAM Paris, France.

Hagège B, Boisse P and Billoët J-L (2005), 'Finite element analyses of knitted composite reinforcement at large strain', *European Journal of Computational Mechanics*, 14 (6–7), 767–776.

Halquist J O, Goudreau G L, Benson D J (1985), 'Sliding interfaces with contact impact in large scale Lagrangian computations', *Comp. Meth. Appl. Engng*., 51, 107-137.

Hsiao S W, Kikuchi N (1999), 'Numerical analysis and optimal design of composite thermoforming process', *Comp. Meth. Appl. Mech. Engrg*., 177, 1–34.

Kawabata S, Niwa M, Kawai H (1973), 'The finite deformation theory of plain weave fabrics part I: The biaxial deformation theory', *J. Textile Inst*., 64 (1), 21–46.

Laine B, Hivet G, Boisse P, Boust F, Lomov S (2005), 'Permeability of the woven fabrics: A parametric study', *Proceedings of the 8th Int.Conf. ESAFORM on Material Forming,* Cluj-Napoca (Roumanie), 2, 995–998.

Lee W, Springer G (1987), 'A model of the manufacturing process of thermoplastic matrix composites', *Journal of Composite Materials*, 21, 1017–1055.

Lomov S V, Stoilova T, Verpoest I (2004), 'Shear of woven fabrics: theoretical model, numerical experiments and full strain measurements', *Proceedings of the Int. Conf ESAFORM 7*, Trondheim, 345–348.

Lomov S V, Bernal E, Ivanov D S, Kondratiev S V, Verpoest I (2005), 'Homogenisation of a sheared unit cell of textile composites: FEA and approximate inclusion model', *European Journal of Computational Mechanics*, 14 (6–7), 709–729.

Long A C, Rudd C D (1994), 'A simulation of reinforcement deformation during the production of preform for liquid moulding processes', *I. Mech. E. J. Eng. Manuf.*, 208, 269–278.

Long A C, Souter B J, Robitaille F (2001), 'Mechanical modelling of in-plane shear and draping for woven and non-crimp reinforcements', *J. of Thermoplastic Composite Materials*, 14, 316–326.

Maison S, Thibout C, Garrigues C, Garcin J L, Payen H, Sibois H (1998), 'Technical developments in thermoplastic composites fuselages', *SAMPLE Journal*, 34 (5), 33–39.

Mark C, Taylor H M (1956), 'The fitting of woven cloth to surfaces', *Journal of Textile Institute*, 47, 477–488.

McBride T M, Chen J (1997), 'Unit-cell geometry in plain-weave fabrics during shear deformations', *Composites Science and Technology*, 57, 3, 345–351.

McGuinness G B, Bradaigh C M O (1997), 'Development of rheological models for forming flows and picture-frame shear testing of fabric reinforced thermoplastic sheets', *Journal of Non-Newtonian Fluid Mechanics*, 73, 1–2, 1–28.

McGuinness G B, Bradaigh C M O (1998), 'Characterisation of thermoplastic composite melts in rhombus-shear: the picture-frame experiment', *Composites Part A*, 29, 1–2, 115–132.

Ó Brádaigh C M, McGuinness G B, Pipes R B (1993), 'Numerical analysis of stresses and deformations in composite materials sheet forming: Central indentation of a circular sheet', *Composites Manufacturing*, 4, (2), 67–83.

Peng X, Cao J (2002), 'A dual homogenization and finite element approach for material characterization of textile composites', *Composites B*, 33, 45–56.

Pickett A K (2002), 'Review of finite element methods applied to manufacturing and failure prediction in composite structures', *Applied Composite Material*, 9, 43–58.

Pickett A K, Creech G, de Luca P (2005), 'Simplified and advanced simulation methods for prediction of fabric draping', *European Journal of Computational Mechanics*, 14 (6–7), 677–691.

Pickett T (2005), 'Modelling drape and impact of textile composites: meso and macro approaches', *Conference Advances in Multi-Scale Modelling of Composite Material Systems and Components*, Monterey, USA, 65–66.

Prodromou A G, Chen J (1997), 'On the relationship between shear angle and wrinkling

of textile composite preforms', *Composites Part A,* 28, 491–503.
Ramgulam R, Potluri P (2005), 'Mechanics of woven fabrics using cruciform elements', *European Journal of Computational Mechanics*, 14 (6–7), 653–676.
Raffel M, Willert C, Kompenhaus J (1998), *Particule Image Velocimetry. A practical guide*, Experimental Fluid Mechanics, Springer Berlin.
Sharma S B, Sutcliffe M P F (2003), 'A simplified finite element approach to draping of woven fabric', *Proceedings of the 6th Int.Conf. ESAFORM on Material Forming*, Salerno, Italy, 887–890.
Simo J C, Fox D D, Rifai M S (1990), 'On a stress resultant geometrically exact shell model. Part 4: Variable thickness shells with trough-the-thickness stretching', *Comp. Meth. in App. Mech. and Engng*, 79, 21–70.
Skordos A, Monroy Aceves C, Sutcliffe M (2005), 'Development of a simplified finite element model for draping and wrinkling of woven material', *Proceedings of the 8th Int.Conf. ESAFORM on Material Forming*, Cluj-Napoca (Romania).
Soulat D, Cheruet A, Youssef M, Boisse P (2006), 'Simulation of continuous fibre reinforced thermoplastic forming using a shell finite element with transverse stress', *Computers and Structures*, 84, 13–14, 888–903.
Sukumar N, Moran B, Belytschko T (1998), 'The natural element method in solid mechanics', *International Journal for Numerical Methods in Engineering*, 43 (5), 839–887.
Tollenaere H, Caillerie D (1998), 'Continuous modelling of lattice structures by homogenization', *Advances in Engineering Software*, 29 (7), 600–705.
Trochu F, Gauvin R, Gao D-M (1993), 'Numerical analysis of the resin transfer molding process by the hinite element method', *Advances in Polymer Technology*, 12 (4), 329–342.
Vacher P, Dumoulin S, Arrieux R (1999), 'Determination of the forming limit diagram from local measurement using digital image analysis', *International Journal of Forming Processes*, 2–4, 395–408.
Van Der Ween F (1991), 'Algorithms for draping fabrics on doubly curved surfaces', *International Journal of Numerical Method in Engineering*, 31, 1414–1426.
Wagoner R, Chenot J L (1996), *Fundamentals of metal forming analysis*, Wiley.
Xue P, Peng X, Cao J (2003), 'A non-orthogonal constitutive model for characterizing woven composites', *Composites Part A*, 34, 183–193.
Yu W R, Pourboghrat F, Chung K, Zamploni M, Kang T J (2002), 'Non-orthogonal constitutive equation for woven fabric reinforced thermoplastic composites', *Composites Part A*, 33, 1095–1105.
Yu X, Ye L, Mai Y-W (2004), 'Finite element spurious wrinkles on the thermoforming simulation of woven fabric reinforced composites', *Proceedings of the Int. Conf ESAFORM 7*, Trondheim, 325–328.
Zouari B, Daniel J L, Boisse P (2006), 'A woven reinforcement forming simulation method influence of the shear stiffness', *Computers and Structures*, 84, 5–6, 351–363.